LBL-37961
UC-411
CONF-9511139--2

Lawrence Berkeley Laboratory
UNIVERSITY OF CALIFORNIA

CHEMICAL SCIENCES DIVISION

To be presented at the XXth International Solvay Conference in Chemistry, Brussels, Belgium, November 28–December 2, 1995, and to be published in the Quantum and Semiclassical Theories of Chemical Reaction Rates I

Photodissociation Spectroscopy and Dynamics of the Vinoxy (CH_2CHO) Radical

D.L. Osborn, H. Choi, and D.M. Neumark

November 1995

Prepared for the U.S. Department of Energy under Contract Number DE-AC03-76SF00098

LBL-37961
UC-411

Photodissociation Spectroscopy and Dynamics of the Vinoxy (CH_2CHO) Radical

David L. Osborn, Hyeon Choi, and Daniel M. Neumark

Department of Chemistry
University of California, Berkeley

and

Chemical Sciences Division
Lawrence Berkeley Laboratory
University of California
Berkeley, California 94720

November 1995

This work was supported by the Director, Office of Energy Research, Office of Basic Energy Sciences, Chemical Sciences Division, of the U.S. Department of Energy under Contract No. DE-AC03-76SF00098.

Photodissociation spectroscopy and dynamics of the vinoxy (CH_2CHO) radical

David L. Osborn, Hyeon Choi, and Daniel M. Neumark

Department of Chemistry, University of California, Berkeley, CA 94720 (USA), and

Chemical Sciences Division, Lawrence Berkeley Laboratory, Berkeley, CA 94720 (USA)

Abstract

The photodissociation spectroscopy and dynamics of the vinoxy (CH_2CHO) radical have been studied using fast beam photofragment translational spectroscopy. The photodissociation cross section over the $B\,^2A'' \leftarrow X\,^2A''$ band is measured, and photofragment translational energy and angular distributions are obtained at several excitation energies. For CH_2CHO, predissociation is observed over the entire band, including several transitions near the band origin which were seen previously in laser-induced fluorescence experiments. Two dissociation channels are seen: CH_3 + CO and H + CH_2CO. The CH_3+ CO channel was investigated in considerable detail and appears to proceed via internal conversion to the CH_2CHO ground state followed by isomerization to CH_3CO and subsequent dissociation. The translational energy distributions for this channel suggest an isomerization barrier in the range of 2 eV with respect to CH_3 + CO products.

Introduction

Photodissociation experiments have become one of the most valuable tools in chemical physics for the purpose of understanding how excited electronic states couple to the dissociation continuum. These experiments, and the theory developed to explain them, have yielded considerable insight into the variety of dynamical processes that occur subsequent to electronic excitation.[1] From these studies, one hopes to obtain bond dissociation energies, chracterize the symmetry of the excited state, measure the product branching ratios, and determine if the excited state undergoes direct dissociation on an excited state surface, predissociation via another excited state, or internal conversion to the ground state followed by "statistical" decay to products.

There are two clear recent trends in photodissociation experiments. One is to perform extremely detailed measurements on systems where the basic photodissociation dynamics are reasonably well understood. As an example, experiments have been reported on CD_3I in which the parent molecule is state-selected and oriented prior to photodissociation;[2] multiphoton ionization of the CD_3 fragment combined with imaging detection yields angular and kinetic energy distributions for each product rotational state. An alternate direction is to apply well-developed photodissociation techniques to larger and/or more complex species, with the goal of seeing what new phenomena appear which are absent in the more commonly studied small model systems. The work of Butler[3] on acetyl halides is a nice example of this; these studies have probed subtle non-adiabatic effects that dramatically affect the product branching ratio.

The approach taken in our laboratory combines both of these trends. Specifically, we have developed a new experiment which allows us to study, for the first time, the photodissociation spectroscopy and dynamics of an important class of molecules: reactive free radicals. This work is motivated in part by the desire to obtain accurate bond dissociation energies for radicals, in order to better determine their possible role in complex chemical mechanisms such as typically occur in combustion or atmospheric chemistry. Moreover, since radicals are open-shell species, one expects many more low-lying electronic states than in closed-shell molecules of similar size and composition. Thus, the spectroscopy and dissociation dynamics of these excited states should, in many cases, be qualitatively different from that of closed shell species.

While one might expect that the techniques developed for photodissociation studies of closed-shell molecules would be readily adaptable to free radicals, this is not the case. A successful photodissociation experiment often requires a very clean source for the radical of interest in order to minimize background problems associated with photodissociating other species in the experiment. Thus, molecular beam photofragment translation spectrosopy, which has been applied to innumerable closed shell species, has been used successfully on only a handful of free radicals. With this problem in mind, we have developed a conceptually different experiment[4] in which a fast beam of radicals is generated by laser photodetachment of mass-selected negative ions. The radicals are photodissociated with a second laser, and the fragments are detected in coincidence with a position and time sensing detector. This detection scheme yields high resolution photofragment energy and angular distributions for each product channel. The negative

ion production scheme insures that only the desired radicals are produced. We have studied several radicals with this experiment during the last few years. In this paper we report new results on the photodissociation spectroscopy and dynamics of the vinoxy radical, CH_2CHO.

The vinoxy radical is an important intermediate in hydrocarbon combustion; it is one of the primary products of ethylene oxidation. The electronic absorption spectrum was obtained by Hunziker,[5] who found two bands with origins at 8000 and 28,760 cm^{-1}. On the basis of *ab initio* calculations by Dupuis,[6] these were assigned to transitions from the $X\,^2A''$ ground state to the $A\,^2A'$ and $B\,^2A''$ states, respectively. The higher energy $B \leftarrow X$ band extends at least to 35,700 cm^{-1}. In Hunziker's experiment, this band shows some partially resolved features near the origin, but little structure remains above 31,200 cm^{-1}. Inoue[7] and Miller[8] have measured laser-induced fluorescence (LIF) spectra of the $B \leftarrow X$ band, and the appearance is very different. These spectra consist of only a few sharp features between the origin and 30,200 cm^{-1}; no fluorescence signal is observed for excitation to the blue of this. The comparison of the absorption and LIF spectra implies that rapid predissociation occurs beyond 30,200 cm^{-1}, thereby quenching any fluorescence. This is consistent with a recent hole-burning study by Gejo et al.[9] Hence, this is an attractive species from the perspective of our photodissociation experiment, since we can examine the competition between predissociation and fluorescence in more detail.

The primary photochemistry of the vinoxy radical is also of interest. Several relatively low-lying dissociation channels are available:[10,11]

$$CH_2CHO \rightarrow CH_3 + CO, \quad \Delta E = 0.05\ eV \qquad (1)$$

$$CH_2CHO \rightarrow H + CH_2CO, \quad \Delta E = 1.45\ eV \qquad (2)$$

$$CH_2CHO \rightarrow CH_2 + HCO, \quad \Delta E = 4.1\ eV \qquad (3)$$

Channel (1), the lowest energy channel, requires a hydrogen shift, while (2) and (3) are simple bond fission channels. Channels (1) and (2) are accessible from all levels of the *B* state, whereas channel (3) can be accessed only at the blue edge of the *B*←*X* band.

Our experiment reveals that *all* levels of the *B* state in CH_2CHO predissociate. We observe dissociation to channels (1) and (2). Kinetic energy distributions at several dissociation energies indicate that CH_3 + CO production takes place following internal conversion to the ground state potential energy surface. These distributions are indicative of a barrier of 1-2 eV along the reaction coordinate to dissociation on the ground state surface. A comparison of our results to photodissociation studies of the acetyl (CH_3CO) radical[12,13] suggests that this barrier corresponds to the isomerization barrier between vinoxy and acetyl on the ground state surface.

Experimental:

The fast beam photodissociation instrument has been described in detail previously.[4] Briefly, a beam of vinoxide (CH_2CHO^-) anions is generated by bubbling O_2 at 3 atm through acetaldehyde at -78° C. The deuterated species (CD_2CDO^-) is made in a similar fashion. The mixture is introduced to the spectrometer through a pulsed molecular beam valve. Ions are generated by means of a pulsed discharge assembly, attached to the faceplate of the valve, through which the gas pulse passes. By firing the discharge just after the valve is open, one forms a variety of ions that cool significantly (~50 K) in the

resulting free jet expansion. The pulsed beam passes through a skimmer, and negative ions in the beam are accelerated up to 8 keV and mass-separated by time-of-flight. The vinoxide ions are then photodetached with an excimer-pumped dye laser. CH_2CHO^- and CD_2CDO^- were photodetached at 663 nm (1.870 eV) and 667 nm (1.859 eV), respectively. These energies are just above the electron affinities[14] of CH_2CHO (1.824 eV) and CD_2CDO (1.818 eV). Remaining ions are deflected out of the beam, leaving a fast pulse of mass-selected vinoxy radicals. These are photodissociated with a second excimer-pumped dye laser. The photofragments are detected with a microchannel plate detector that lies on beam axis, 1 m downstream from the dissociation region. A blocking strip across the center of the detector prevents parent radicals from reaching the detector, whereas those photofragments with sufficient kinetic energy miss the beam block and strike the detector. These fragments are generally detected with high efficiency (up to 50%) due to their high laboratory kinetic energy.

Three types of measurements were performed in this study. First, photodissociation cross sections were measured, in which the total photofragment yield was measured as a function of dissociation photon energy. In these experiments, the electron signal generated by the microchannel plates is collected with a flat metal anode, so that only the total charge per laser pulse is measured. The beam block is 3 mm wide for these measurements.

To perform photodissociation dynamics experiments, the dissociation laser is tuned to a transition where dissociation occurs. Most of the dynamics studies described here employ a time-and-position sensing photofragment coincidence detection scheme[15] in

which a dual wedge-and-strip anode[4] is used to collect the electron signal from the microchannel plates. For each dissociation event, we measure the distance R between the two fragments on the detector, the time delay τ between their arrival, and the individual displacements of the two fragments, r_1 and r_2 from the detector center. From this we obtain the center-of-mass recoil energy, E_T, the scattering angle with respect to laser polarization, θ, and the two photofragment masses m_1 and m_2, via:

$$m_1 / m_2 \equiv r_2 / r_1$$

$$\theta = \tan^{-1}\left(\frac{R}{v_0\tau}\right) \qquad (4)$$

$$E_T = E_0 \cdot \left(\frac{m_1 m_2}{M}\right) \cdot \frac{[(v_0\tau)^2 + R^2]}{l^2} \cdot \left(1 + 2\frac{(m_2 - m_1)v_0\tau}{Ml}\right)$$

Here E_0 and v_0 are the ion beam energy and velocity, respectively, and l is the flight length from the photodissociation region to the detector. An 8 mm wide beam block is used for these measurements; a narrower block results in crosstalk between the two halves of the anode.

The coincidence scheme works very well so long as the $m_1/m_2 \leq -5$, and is thus quite suitable for channel (1). However, for channel (2), the fragment mass discrepancy is too large to perform this type of measurement. The recoil velocity of the heavy fragment is too small to clear the beam block, and the laboratory energy of the H (or D) atom is so low that their detection efficiency drops considerably. Since either of these effects makes coincidence measurements difficult, if not impossible, we performed a somewhat less complex experiment to detect and analyze channel (2). The flat anode configuration of the detector (with the 3 mm beam block) was used, and we simply measure the time-of-flight distribution of all fragments at the detector. This was used previously to measure the

kinetic energy release in NCO photodissociation.[16] For the present study, we only investigated CD_2CDO since the fragment mass ratio for channel (2) is smaller than for CH_2CHO. As will be seen below, our ability to measure the kinetic energy distribution for channel (1) via the coincidence scheme allows us to subtract the contribution of this channel from the time-of-flight measurement. This enables us to isolate the contribution of channel (2) to this measurement.

Results:

Photodissociation cross sections for CH_2CHO and CD_2CDO are shown in Figure 1. Both spectra consist of sharp, extended vibrational progressions indicative of predissociation. A comparison of Figure 1 with the LIF and absorption spectra[5,7,8] shows that we observe predissociation all the way to the origin of the $B \leftarrow X$ band; this is labeled peak 1 in Figure 1. We observe photodissociation over the entire range of the absorption band. However, peaks 1-7 are the only peaks seen in the LIF spectrum. Peaks 1, 2, 5, and 6 are particularly prominent in the LIF spectrum; the latter three peaks are assigned by Yamaguchi[17] to the 9_0^1, 8_0^1, and 7_0^1 transitions involving the C-C-O bend, C-C stretch, and CH_2 rock, respectively. While peak 1 is the most intense peak in the LIF spectrum, it is the weakest of the four in Figure 1. This shows that the competition between LIF and predissociation tilts sharply in favor of the latter even over the small energy range spanned by peaks 1-4.

Photofragment coincidence data were taken at several of the peaks in Figure 1. Mass analysis of the fragments showed that only coincidences corresponding to channel 1,

CH_3 + CO (or CD_3 + CO) were seen at all dissociation wavelengths examined. As discussed previously, the time and position data yield a coupled translational energy and angular distribution $P(E_T,\theta)$, which can be written as:

$$P(E_T,\theta) = P(E_T)\cdot(1+\beta(E_T)\cdot P_2(\cos(\theta)). \qquad (5)$$

Here $P(E_T)$ is the angle-independent translational energy distribution, and $\beta(E_T)$ is the (energy-dependent) anisotropy parameter, with $-1\leq\beta\leq2$.

Figure 2 shows the $P(E_T)$ distributions for CH_2CHO at the four dissociation energies indicated by peaks A-D in Figure 1. The distributions all peak at nonzero translational energy. The most striking feature of Figure 2 is the insensitivity of the $P(E_T)$ distributions to photon energy; only a very small shift towards higher E_T is seen over the entire energy range that was probed. The $P(E_T)$ distributions for CD_2CDO photodissociation are similar and again show little variation with photon energy. Figure 3 shows the average anisotropy parameter at each photon energy for both CH_2CHO photodissociation. This shows that the angular distributions are isotropic ($\beta\cong0$) at *B* state excitation energies below 1000 cm^{-1}, but for higher energies we find β in the range of 0.4-0.5. Note that the angular distribution becomes anisotropic in the energy range where fluorescence is quenched.

Finally, the photofragment time-of-flight distribution for CD_2CDO photodissociation at 31,980 cm^{-1} is shown in Figure 4. This will be analyzed in detail in the next section, but for now it suffices to point out that the wings in the distribution are from D atoms, therefore indicating that photodissociation channel (2) to D + CD_2CO is indeed occurring.

Discussion:

A. CH_3 + CO channel

The shape of the $P(E_T)$ distributions for channel (1) and their insensitivity to excitation energy is characteristic of statistical decomposition over a barrier. Distributions of this type are often seen in infrared multiphoton dissociation of molecules in which there is a barrier to product formation on the ground state potential energy surface,[18] and also for electronic excitation in which internal conversion to the ground state occurs prior to dissociation.[19] The rationale for these distributions is that dissociation is statistical up until the top of the barrier. At this point, the most likely trajectories have nearly zero translational energy since this maximizes the number of vibrational states perpendicular to the reaction coordinate that can be populated. This is true regardless of the total excitation energy, provided dissociation is sufficiently slow so that energy randomization can occur. However, once the barrier is traversed, the photofragments move apart too quickly for the newly available energy to be fully randomized, so that the translational energy distribution peaks at some fraction of the barrier height, typically 40-80%.

It therefore appears that channel (1) occurs via internal conversion from the initially excited *B* (^{2}A") state to the *X* (^{2}A") state, and that the peaking of the $P(E_T)$ distributions around 1 eV translational energy is caused by a barrier between 1.2-2.4 eV on the ground state potential energy surface. We now consider the location of this barrier along the reaction coordinate. Internal converision from the *B* state will result in highly

vibrationally excited CH_2CHO. In order to dissociate to CH_3 + CO, this species must first isomerize to the acetyl radical, CH_3CO, and then break the C-C bond in this radical. One certainly expects a barrier to be associated with isomerization, and the photodissociation experiments by North et al.[12] indicate that there is a barrier associated with breaking the C-C bond in the acetyl radical. Hence, there should be two barriers along the reaction coordinate as shown in Figure 5.

Given this reaction coordinate, we now want to consider which barrier is responsible for the maximum in the $P(E_T)$ distributions. In North's experiment, acetyl chloride (CH_3COCl) is photodissociated at 248 nm to yield Cl + CH_3CO. Time-of-flight analysis of the photofragments shows that the CH_3CO radical undergoes secondary dissociation when it contains more than 17 ± 1 kcal/mol of internal energy, indicating that this is the barrier height for the reaction $CH_3CO \rightarrow CH_3$ + CO. This reaction is endothermic by only 11 kcal/mol, however, so the barrier is 6 kcal/mol (0.26 eV) above CH_3+ CO products. These energetics are consistent with recent *ab initio* calculations by Deshmukh et al.[13] Thus, according to our model for the dissociation, this barrier *cannot* be responsible for the peak at 1 eV in the $P(E_T)$ distributions, since one generally expects only a fraction of the barrier height to manifest itself in this manner.

This suggests that the peak in the translational energy distributions reflects the isomerization barrier in Figure 5. If this is so, the barrier should lie 1-2 eV above the products, and preliminary *ab initio* calculations in our group indicate that this is a reasonable range of values. Our interpretation implies that once isomerization occurs, the resulting energized CH_3CO falls apart very rapidly, before energy randomization can

happen. Otherwise, the smaller barrier would determine the product translational energy distributions. This is what happens in the infrared multiphoton dissociation (IRMPD) of CH_3NO_2, where the $CH_3O + NO$ product channel is formed by isomerization to CH_3ONO followed by dissociation with no exit barrier.[18] The translational energy distribution peaks at zero, consistent with the dynamics being determined by the absence of an exit barrier for dissociation rather than the isomerization barrier, which lies about 0.6 eV above the products. However, the CH_3ONO well lies 1.8 eV below $CH_3O + NO$, whereas the CH_3CO well is only 0.7 eV deep relative to the exit barrier to dissociation. In addition, the ratio of the excitation energy to the well depth is much higher in our experiment than in the IRMPD study (>5 vs. <1). Thus, once isomerization to CH_3CO occurs, dissociation may be so rapid that the well does not noticeably affect the final state dynamics. Alternatively, concerted elimination to $CH_3 + CO$ may occur at the top of the isomerization barrier, in which case the resulting reaction path would not pass through the CH_3CO well (and over the second barrier) at all. Clearly, the detailed dissociation on the ground state surface will have to be examined in more detail once a reasonable potential energy surface is developed.

At excitation energies close to the band origin, fluorescence still competes effectively with dissociation. We interpret this to mean that the initial internal conversion to the ground state is sufficiently slow at these energies that fluorescence is competitive. However, it appears that as the vibrational energy in the *B* state increases, internal conversion becomes so rapid that fluorescence is completely quenched. This is consistent with the angular distributions. These are isotropic ($\beta \equiv 0$) for those transitions that exhibit

fluorescence, but anisotropic distributions occur at higher excitation energies where the fluorescence is quenched, indicating the lifetime with respect to dissociation has dropped substantially. Thus, it is the early time dynamics following excitation that determine the outcome of the competition between fluorescence and dissociation.

The rather abrupt change in the relative quantum yields for fluorescence *vs.* dissociation is of considerable interest. A possible mechanism has been proposed by Yamaguchi[20] based on *ab initio* calculations of the various CH_2CHO excited state energies as a function of the C-C torsional angle. He finds that energy of the $B(^2A")$ state rises only slightly (3300 cm^{-1}) over the entire torsion angular range. In contrast, the $A(^2A')$ state, which is well separated in the planar geometry, approaches to within 2200 cm^{-1} of the *B* state at a geometry where the planes CH_2 and CHO groups are perpendicular. The implication here is that, with minor adjustments, one can imagine an intersection between the two states at relatively low excitation energy of the *B* state, and this is what promotes the abrupt increase in the internal conversion rate with energy. Our results are certainly consistent with this if one views internal conversion to the *A* state as the rate-limiting component in a two step internal conversion process that finishes on the ground electronic state.

B. D + CD_2CO channel

The time-of-flight distribution in Figure 4 has contributions from channels (1) and (2). However, we know the detailed form of the energy and angular distribution for channel (1) from our photofragment coincidence measurements. The contribution from

the CH_3 and CO fragments data in Figure 4 can then be determined by using a Monte Carlo simulation to calculate the fragment time-of-flight distribution from channel (1) based on the known energy and angular distribution; this procedure, which averages over all relevant experimental parameters, is described in more detail in Ref. 16. The result in shown as the dotted (?) line in Figure 4. The comparison of the simulation with the data shows that channel (2) is responsible for the far wings of the distribution (from the D atoms) *and* the sharp peak at the center. This latter feature must come from CD_2CO which barely recoils out of the beam, and therefore misses the smaller beam block used in this detector configuration.

The inset to Figure 4 shows a center-of-mass translational energy distribution for channel (2) that, when run through our Monte Carlo program, generates the time-of-flight distribution shown by the dashed lines in Figure 4. This distribution, when added to that for CH_3 + CO, adequately reproduces the total experimental time-of-flight distribution. We can therefore learn about the dynamics of channel (2), although not in as much detail as channel (1). The translational energy distribution for channel (2) also peaks away from zero, implying that there is an exit channel barrier to hydrogen atom loss. This is not unusual for the ground state dissociation of a radical to a radical (D) + closed-shell species (ketene). Although we do not have data for channel (2) at the whole series of excitation energies as we do for channel (1), it is reasonable to expect that channel (2) also proceeds by internal conversion to the ground state followed by statistical decomposition over a barrier.

It is clearly of interest to know the branching ratios between the two channels. Unfortunately, this is complicated by two factors. First, we only observe CD_2CO fragments near the high energy limit of the translational energy distribution; slower fragments strike the beam block and are not detected. This effect is taken into account in the Monte Carlo generation of a time-of-flight spectrum, but it does means that the low energy portion of the translational energy distribution is poorly determined. Secondly, the detection efficiency of the D atoms is considerably lower than that of the heavy fragments, but we do not know exactly how low. We estimate the detection efficiency to be between 1-10%; the true branching ratio clearly depends on this value. It does appear that channel (2) is a major channel, contributing at least 50% to the total fragmentation. A more detailed analysis is currently underway to better quantify this channel.

Conclusions

This work represents the first study of the photodissociation dynamics of the vinoxy radical. We observe predissociation over the entire $B\,^2A'' \leftarrow X\,^2A''$ band of CH_2CHO, including the origin at 28,760 cm^{-1}. Two dissociation channels are observed: $CH_3 + CO$, and $H + CH_2CO$. Translational energy distributions for the $CH_3 + CO$ channel are largely independent of excitation energy, indicating that this channel is likely due to statistical decomposition on the vinoxy ground state potential energy surface. The translational energy distributions all peak near $E_T = 1$ eV, and we believe this is indicative of the isomerization barrier for conversion of vinoxy (CH_2CHO) to the acetyl radical (CH_3CO) prior to dissociation. A comparison of our results with previous laser-induced

fluorescence work on CH_2CHO shows that predissociation dominates over fluorescence at excitation energies > 1000 cm^{-1} above the band origin. This is indicates a greatly increased internal conversion rate above this energy, possibly due to another excited state of vinoxy intersecting the $B\,^2A''$ state.

The results presented here show that our instrument can also be used to investigate dissociation channels in which the mass disparity of the two fragments is very large, namely the $H + CH_2CO$ channel; the study of this channel was facilitated by using CD_2CDO. Although the dynamics of this channel cannot be elucidated at the same level of detail as the $CH_3 + CO$ channel, our ability to study it at all represents an important extension of the capabilities of the instrument.

Acknowledgments

This research is supported by the Director, Office of Energy Research, Office of Basic Energy Sciences, Chemical Sciences Division, of the U. S. Department of Energy under Contract No. DE-AC03-76SF00098.

References

[1] R. Schinke, *Photodissociation Dynamics* (Cambridge University Press, Cambridge, 1993).

[2] J. W. G. Mastenbroek, C. A. Taatjes, K. Mauta, M. H. M. Janssen, and S. Stolte, J. Phys. Chem. **99**, 4360 (1995).

[3] M. D. Person, P. W. Kash, and L. J. Butler, J. Chem. Phys. **97**, 355 (1992).

[4] R. E. Continetti, D. R. Cyr, D. L. Osborn, D. J. Leahy, and D. M. Neumark, J. Chem. Phys. **99**, 2616 (1993); D. J. Leahy, D. L. Osborn, D. R. Cyr, and D. M. Neumark. J. Chem. Phys. **103**, 2495 (1995).

[5] H. E. Hunziker, H. Kneppe, and H. R. Wendt, J. Photochem. **17**, 377 (1981).

[6] M. Dupuis, J. J. Wendoloski, and W. A. Lester, Jr., J. Chem. Phys, **76**, 488 (1982).

[7] G. Inoue and H. Akimoto, J. Chem. Phys. **74**, 425 (1981).

[8] L. F. DiMauro, M. Heaven, and T. A. Miller, J. Chem. Phys. **81**, 2339 (1984).

[9] T. Gejo, M. Takayanagi, T. Kono, and I. Hanazaki, Chem. Lett. 2065 (1993).

[10] S. G. Lias, J. E. Bartmess, J. F. Liebman, J. L. Holmes, R. D. Levin, and W. G. Mallard, J. Phys. Chem. Ref. Data **17**, Supplement No. 1 (1988).

[11] C. W. Bauschlicher, Jr., J. Phys. Chem. **98**, 2564 (1994).

[12] S. North, D. A. Blank, and Y. T. Lee, Chem. Phys. Lett. **224**, 38 (1994).

[13] S. Deshmukh, J. D. Myers, S. S. Xantheas, and W. P. Hess, J. Phys. Chem. **98**, 12535 (1994).

[14] R. D. Mead, K. R. Lykke, W. C. Lineberger, J. Marks, and J. I. Brauman, J. Chem. Phys. **81**, 4883 (1984).

[15] D. P. DeBruijn and J. Los, Rev. Sci. Instrum. **53**, 1020 (1982).

[16] D. R. Cyr, R. E. Continetti, R. B. Metz, D. L. Osborn, and D. M. Neumark, J. Chem. Phys. **97**, 4937 (1992).

[17] M. Yamaguchi, T. Momose, and T. Shida, J. Chem. Phys. **93**, 4211 (1990).

[18] A. M. Wodtke, E. J. Hintsa, and Y. T. Lee, J. Phys. Chem. **90**, 3549 (1986), and references therein.

[19] X. Zhao, R. E. Continetti, A. Yokoyama, E. J. Hintsa, and Y. T. Lee, J. Chem. Phys. **91**, 4118 (1989).

[20] M. Yamaguchi, Chem. Phys. Lett. **221**, 531 (1994).

Figure Captions

Figure 1: Photodissociation cross section of CH_2CHO (top) and CD_2CDO (bottom). Peaks 1-7 are the only features seen in the laser-induced fluorescence spectrum of CH_2CHO (Ref. 8).

Figure 2: Translational energy distributions $P(E_T)$ for $CH_2CHO \rightarrow CH_3 + CO$ taken at four dissociation energies corresponding to peaks A-D in Figure 1.

Figure 3: Anisotropy parameter β for $CH_2CHO \rightarrow CH_3 + CO$ at several dissociation energies.

Figure 4: Photofragment time-of-flight spectrum for CD_2CDO excited at 31,980 cm^{-1}, including experimental results, contributions from $D + CD_2CO$ and $CD_3 + CO$ channels, and total simulated spectrum. The $CD_3 + CO$ contribution is obtained from an independent measurement of the energy and angular distribution at this energy using the photofragment coincidence detection scheme. The inset shows the translational energy distribution for the $D + CD_2CO$ channel (with $\beta = 1.2$) used to simulate the contribution of this channel to the time-of-flight spectrum.

Figure 5: Energetics for CH_2CHO dissociation, including qualitative picture of the reaction coordinate for $CH_3 + CO$ production on ground state potential energy surface. See text for discussion of barrier heights.

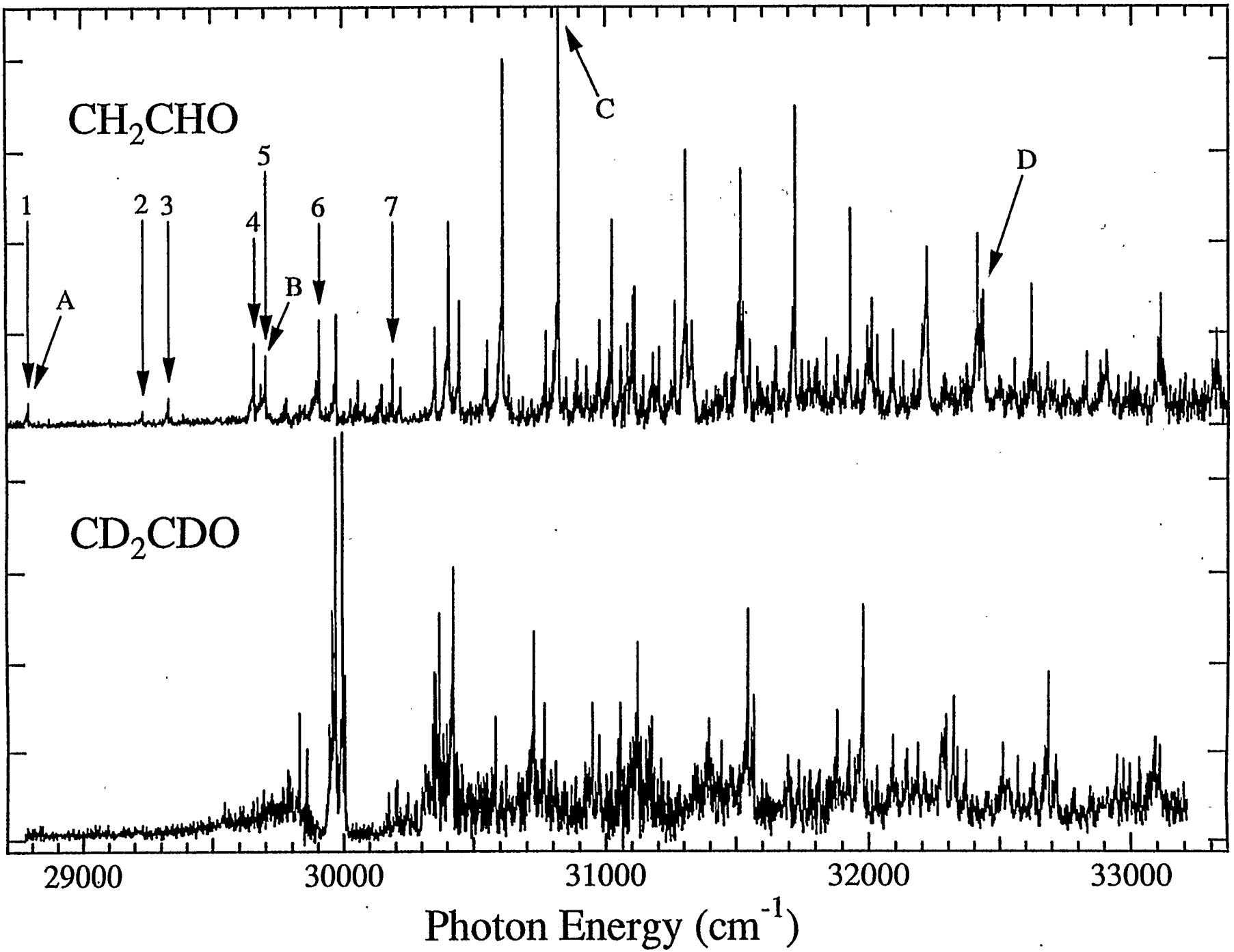
CH2CHO
CD2CDO
1
2
3
4
5
6
7
A
B
C
D
29000
30000
31000
32000
33000
Photon Energy (cm-1)

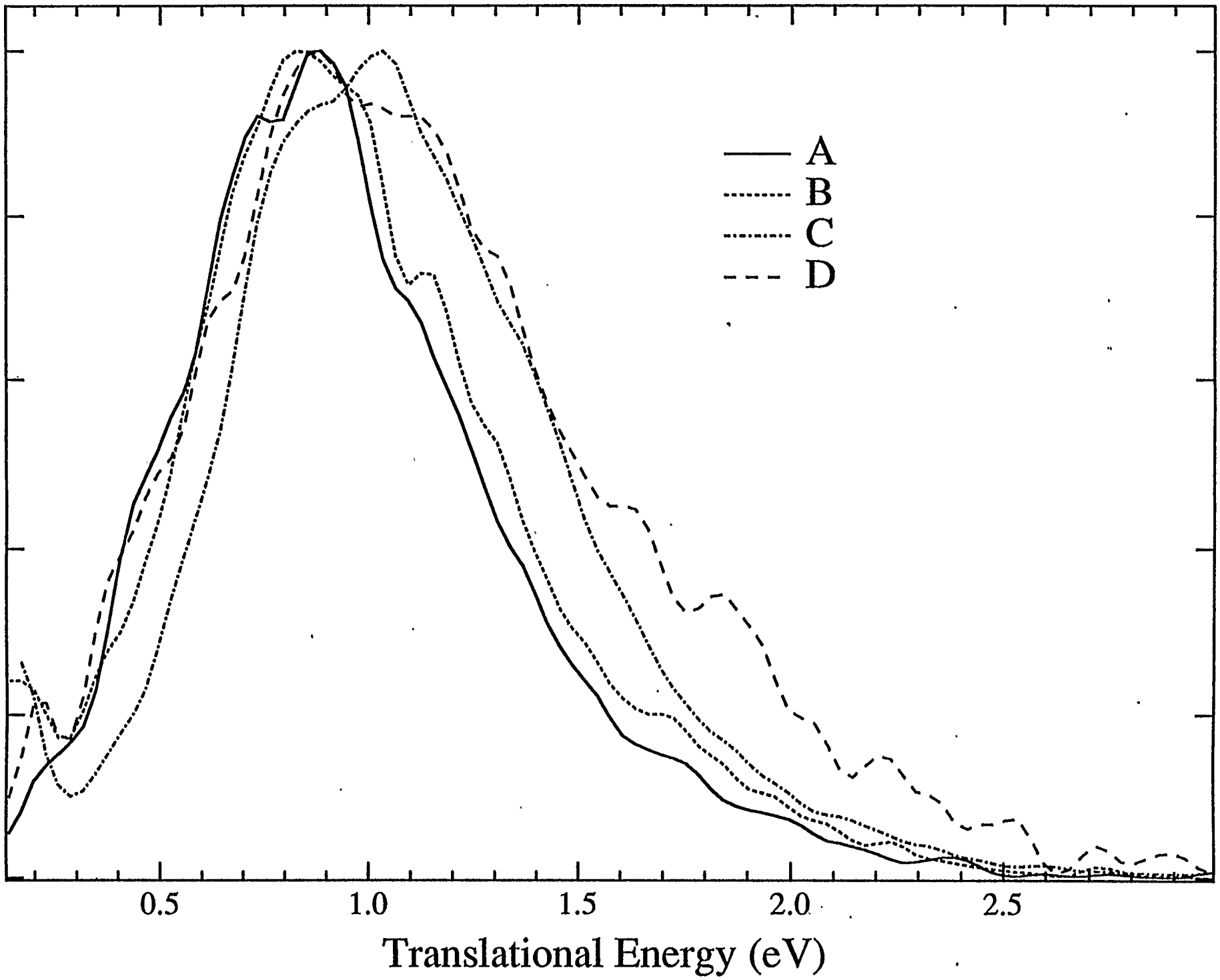
A
B
C
D
0.5
1.0
1.5
2.0
2.5
Translational Energy (eV)

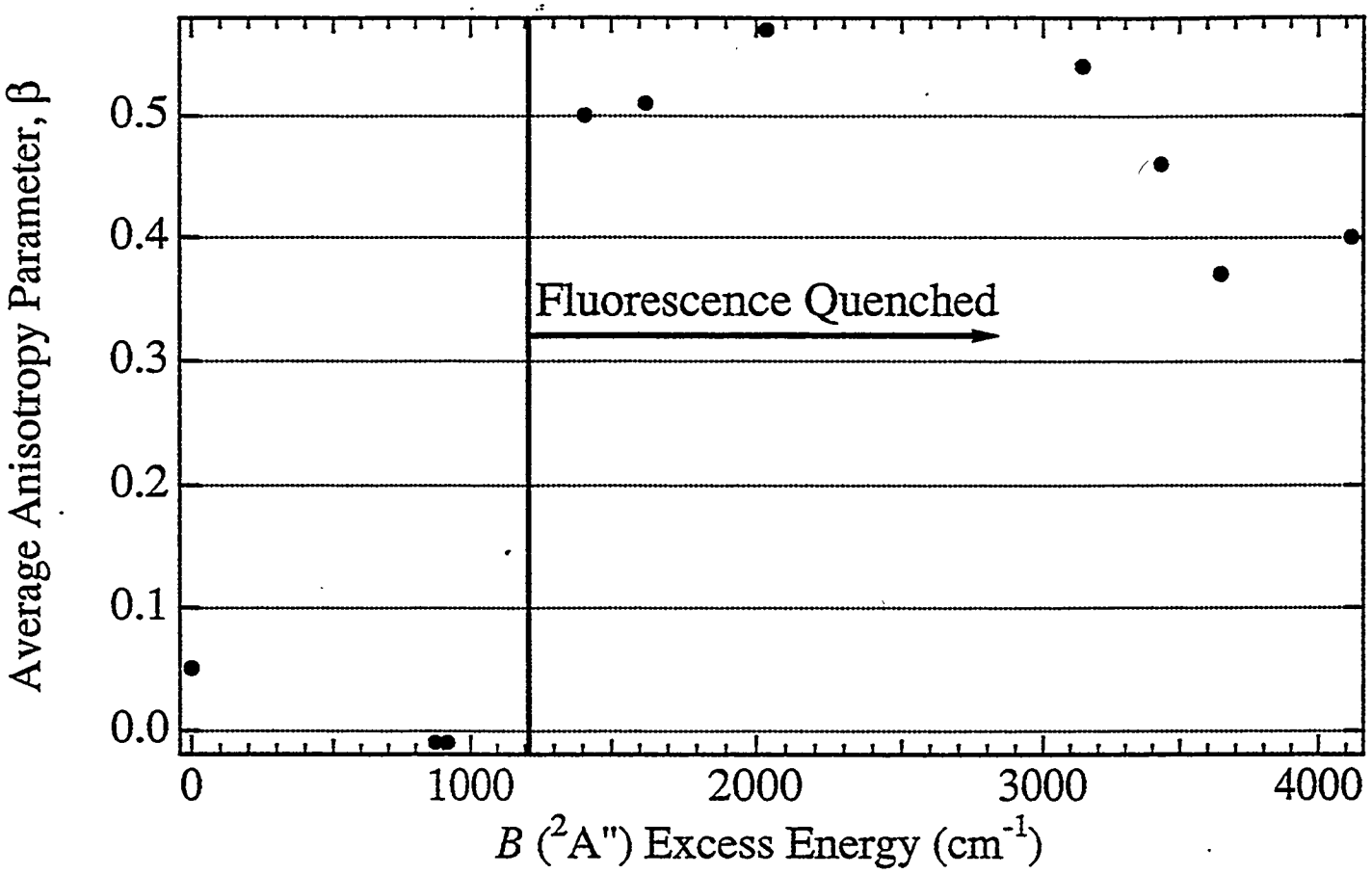
Average Anisotropy Parameter, β
0.0
0.1
0.2
0.3
0.4
0.5
Fluorescence Quenched
0
1000
2000
3000
4000
B (2A") Excess Energy (cm-1)

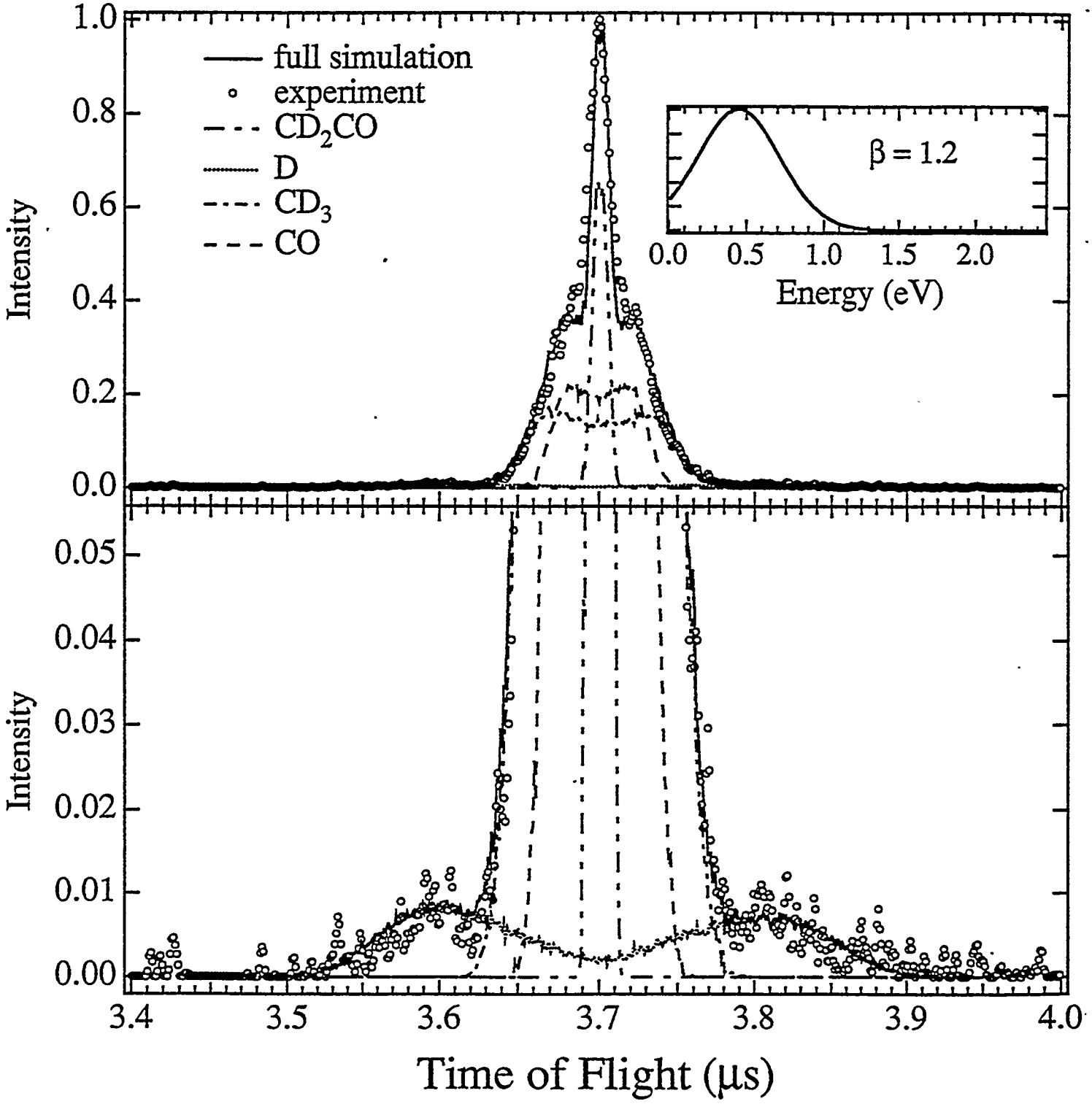
full simulation
experiment
CD2CO
D
CD3
CO
β = 1.2
Energy (eV)
Intensity
Intensity
Time of Flight (μs)

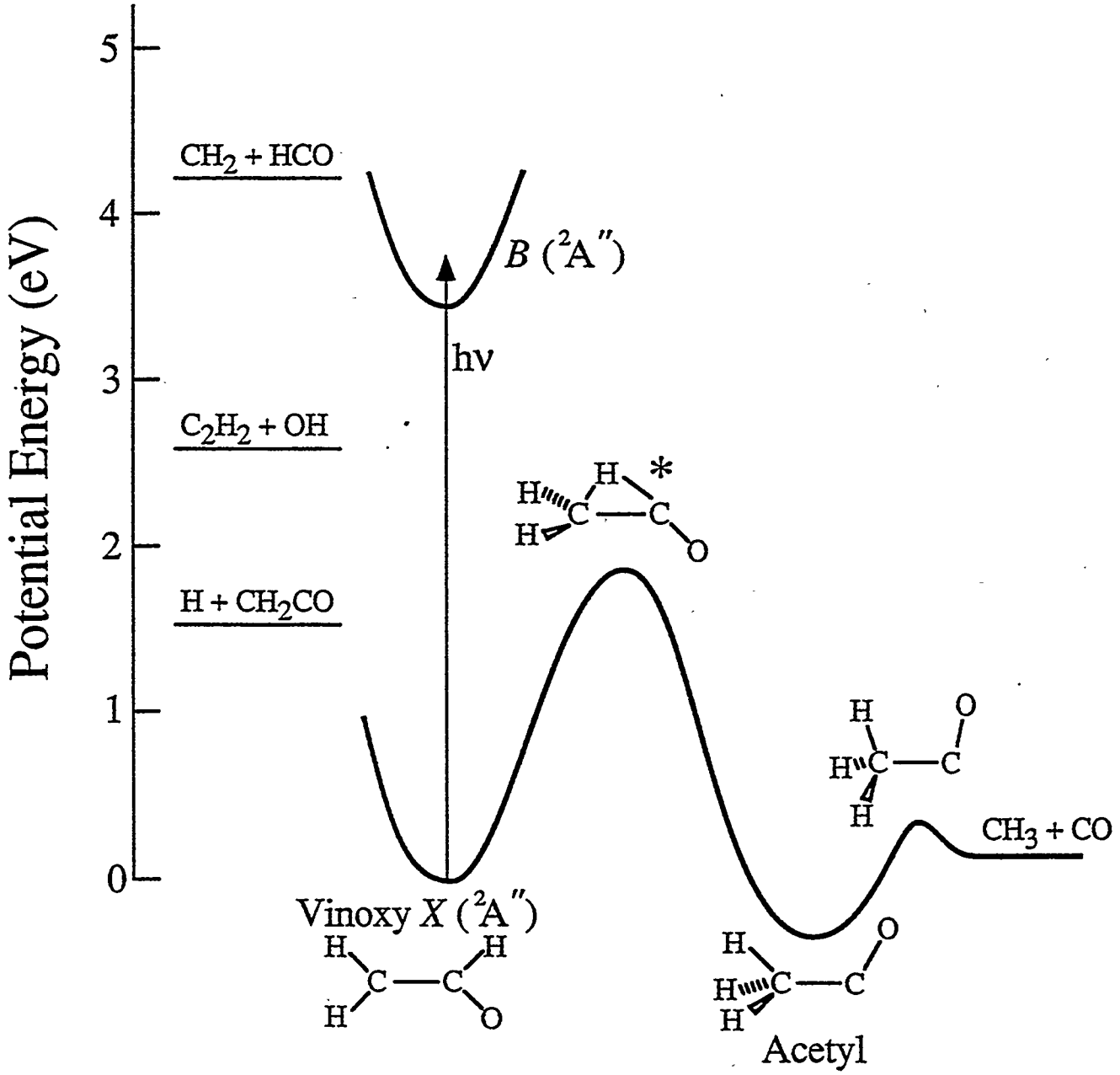
Potential Energy (eV)
5
4
3
2
1
0
CH2 + HCO
C2H2 + OH
H + CH2CO
B (2A″)
hν
Vinoxy X (2A″)
CH3 + CO
Acetyl